Dynamics of H2 Eley-Rideal abstraction from W(110): Sensitivity to the representation of the molecule-surface potential

R. Pétuya, P. Larrégaray, C. Crespos, H. F. Busnengo, and A. E. Martínez

Citation: The Journal of Chemical Physics **141**, 024701 (2014); doi: 10.1063/1.4885139
View online: http://dx.doi.org/10.1063/1.4885139
View Table of Contents: http://scitation.aip.org/content/aip/journal/jcp/141/2?ver=pdfcov
Published by the AIP Publishing

Dynamics of H_2 Eley-Rideal abstraction from W(110): Sensitivity to the representation of the molecule-surface potential

R. Pétuya,[1,2,a)] P. Larrégaray,[1,2] C. Crespos,[1,2] H. F. Busnengo,[3] and A. E. Martínez[3]
[1]*Université de Bordeaux, ISM, CNRS UMR 5255, 33405 Talence Cedex, France*
[2]*CNRS, ISM, UMR5255, F-33400 Talence, France*
[3]*Instituto de Física Rosario (IFIR) CONICET-UNR. Ocampo y Esmeralda (2000) Rosario, Argentina*

(Received 13 January 2014; accepted 12 June 2014; published online 8 July 2014)

Dynamics of the Eley-Rideal (ER) abstraction of H_2 from W(110) is analyzed by means of quasi-classical trajectory calculations. Simulations are based on two different molecule-surface potential energy surfaces (PES) constructed from Density Functional Theory results. One PES is obtained by fitting, using a Flexible Periodic London-Eyring-Polanyi-Sato (FPLEPS) functional form, and the other by interpolation through the corrugation reducing procedure (CRP). Then, the present study allows us to elucidate the ER dynamics sensitivity on the PES representation. Despite some sizable discrepancies between both H+H/W(110) PESs, the obtained projectile-energy dependence of the total ER cross sections are qualitatively very similar ensuring that the main physical ingredients are captured in both PES models. The obtained distributions of the final energy among the different molecular degrees of freedom barely depend on the PES model, being most likely determined by the reaction exothermicity. Therefore, a reasonably good agreement with the measured final vibrational state distribution is observed in spite of the pressure and material gaps between theoretical and experimental conditions. © *2014 AIP Publishing LLC*. [http://dx.doi.org/10.1063/1.4885139]

I. INTRODUCTION

The interaction of hydrogen with metal surfaces is of great importance in several domains of research like heterogeneous catalysis, hydrogen storage, plasma physics, etc. In particular, the (H+H_2)/W system is of current technological interest in the context of the ITER experimental fusion reactor,[1–3] as tungsten is the main candidate for use in the divertors of the tokamaks. More generally, the many elementary processes that take place in the (H+H_2)/W interface are highly relevant, and remain a *hot topic* after almost a century of intense research.[4]

A tungsten surface exposed to a gas of atomic and/or molecular hydrogen will be quickly covered by H atoms. Then, an impinging H atom coming from the gas phase (named in the following *projectile*) can react with a second H atom adsorbed on the surface (named *target*) to form a desorbing H_2 molecule. The mechanism through which this molecular recombination process takes place in a quasi-unique collision is known as Eley-Rideal (ER).[5] The ER mechanism is often considered as a short time process which prevents a sizable energy exchange between the impinging atom and the surface.

The total energy (internal plus translational) of H_2 molecules formed through the ER mechanism is $\sim D_{H_2} - E_H + E_{proj}$, where D_{H_2} is the binding energy of H_2, E_H is the H adsorption energy (for metal surfaces, 2.4 eV $\lesssim E_H \lesssim$ 2.9 eV), and E_{proj} is the initial kinetic energy of the *projectile*. Thus, the total energy of the nascent molecules varies between E_{proj}+1.85 eV and E_{proj}+2.35 eV, depending on the metal surface. This energy is distributed into translational and internal degrees of freedom, in fractions that depend on the dynamics of the ER process. Thus, to predict/understand the rovibrational-state population distribution of H_2 usually measured for (H+H_2) mixtures in contact with a metal surface,[6–10] molecular dynamics simulations of the ER abstraction process are required.

The dynamics of ER abstraction using quasi-classical trajectories (QCT) has been extensively studied during the last 15 years.[11–26] Results of classical trajectory calculations have been found in reasonable agreement with those of quantum scattering simulations for ER abstraction involving hydrogen atoms in reduced dimension models.[12,13,20,23,25–36] Early dynamical studies of the H+H/W ER process made use of two-dimensional (2D) model potential energy surfaces (PES), depending on the altitude of the molecule above the surface and the H-H distance, representing only a collinear geometry where the *projectile* impinges on top of the *target* atom.[11,37] More recently, Rutigliano and Cacciatore[38] investigated the ER abstraction process for H+H/W(100) by using a tight binding approximation for the PES[39,40] that allowed them to consider explicitly not only the six degrees of freedom of the H_2 but also the dynamical coupling with tungsten phonons. Still, a word of caution must be given about the accuracy of the PES employed in the latter study since it predicts the fourfold hollow site as the most stable for H adsorption, in contrast with experiments[41] and Density Functional Theory (DFT) calculations[42] for which the lowest energy adsorption site at low H coverage is the bridge site. To what extent such an error in the PES might affect the outcome of the ER dynamics and in particular, the rovibrational-state distribution of the nascent H_2 molecules, is unclear.

a)Electronic mail: r.petuya@ism.u-bordeaux1.fr

Unfortunately, the very small cross sections of the H+H ER process on metal surfaces (<1 Å^2)[12,14,20,21,25,43–46] hamper the use of *Ab Initio* Molecular Dynamics (AIMD) simulations[47–51] that circumvent the errors of any PES-parametrization method. Therefore, studies of the sensitivity to the PES parametrization of the ER dynamics are desirable. Accordingly, in this work we report results of quasi-classical trajectory (QCT) simulations of the H+H/W(110) ER abstraction process based on two PESs constructed from DFT total energy data. One of the PESs (hereafter referred to as FPLEPS) is a result of a global analytical fitting[52,53] using a generalization[54–56] of the London-Eyring-Polanyi-Sato (LEPS) function[57–59] widely used in the past to investigate H+H ER abstraction processes on metal surfaces.[12,14,20,21,25,43,44,46] The other PES (hereafter referred to as CRP) has been obtained by interpolation using the corrugation reducing procedure[60] which has been widely used[42,49,60–74] and successfully gauged against AIMD results[49,75] of dissociative adsorption probabilities but scarcely used to investigate ER abstraction processes. It has to be mentioned that CRP has already been used in the context of recombination process but for modeling the Langmuir-Hinshelwood mechanism (LH),[76] which can be seen as the reverse mechanism of dissociative adsorption. In consequence CRP models determined for dissociative adsorption can be used straightforwardly without any additional data. As detailed later in the text, the simulation of ER mechanism is more demanding assuming that more configuration space data are required (atomic configurations corresponding to ER entrance channel has to be added in the CRP interpolation scheme). The most common PES determination methods used in gas-surface dynamics studies have been recently reviewed by Gamallo *et al.* (see Ref. 53 and references therein). Through the comparison of these PESs obtained with two types of parametrization methods (fitting procedure vs numerical interpolation scheme), and of the corresponding QCT results, we analyze the influence of the PES topology on the total cross sections and the final-state population distribution of H_2 molecules formed through ER reactions on W(110).

The paper is organized as follows. In Sec. II, we briefly compare the main properties of the FPLEPS and the CRP PESs. In Sec. III, we present the results of QCT simulations of the H+H/W(110) ER abstraction process and we compare them with available experimental data. Finally, in Sec. IV, we summarize the conclusions of our study.

II. THE PESS FOR H+H/W(110)

To investigate the influence of the PES topology on the usual dynamical observables of interest for the ER process (i.e., the total cross section and the distribution of the total energy into the various degrees of freedom of the nascent molecules), two different model PESs have been used in our simulations. Both PESs have been built to accurately reproduce a large set of DFT total energies for the H+H/W(110) system by means of a fitting procedure in the case of the FPLEPS, and numerical interpolation in the case of the CRP. The PESs reproduce properly the most stable atomic adsorption configuration located very close to the hollow

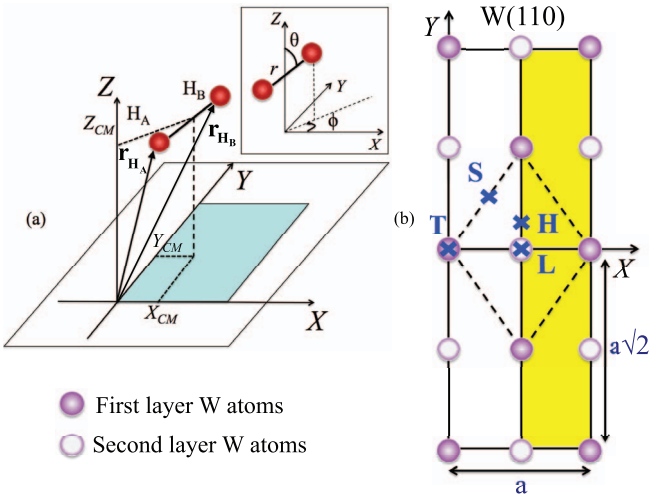

FIG. 1. (a) Definition of the atomic and molecular coordinates employed in this work. (b) W(110) surface unit cell with definition of some surface sites (a = 3.17 Å is the lattice constant of bulk W): T, top (X=0, Y=0); L, long bridge (X=a/2, Y=0); S, short bridge (X=a/4, Y=a$\sqrt{2}$/4); and H, threefold hollow (X=a/2, Y=a$\sqrt{2}$/8). The yellow area represents the region where we have carried out the sampling of the (X, Y) initial position of the *projectile* in the QCT calculations.

site (see Fig. 1), $X_{ads} = a/2 = 1.585$ Å, $Y_{ads} = 0.145a\sqrt{2} = 0.65$ Å, $Z_{ads} = 1.07$ Å, as well as the DFT chemisorption energy of 3.06 eV. Details about the DFT calculations and the parametrization procedures employed are given in the Appendix. The definition of the coordinates used to describe the atom- and molecule-surface systems throughout this work as well as a schematic representation of the W(110) surface are shown in Fig. 1.

Figure 2 illustrates the topology of both PESs (FPLEPS: upper panels, and CRP: lower panels) by representing

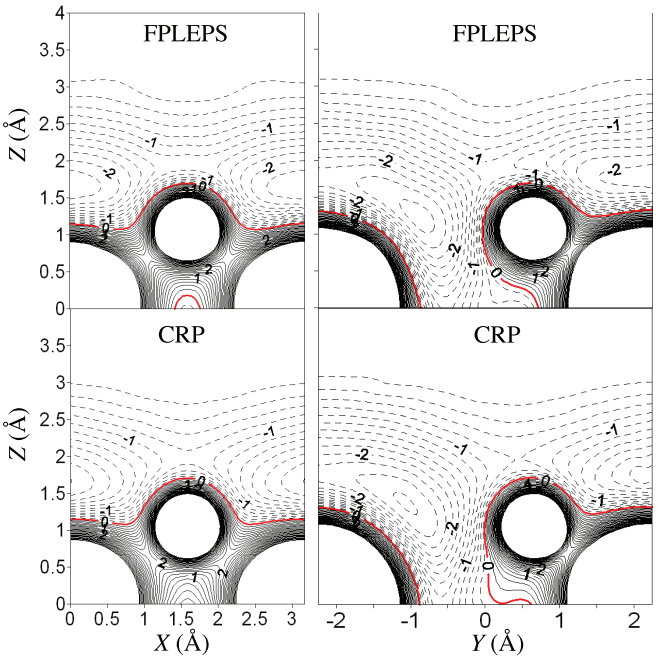

FIG. 2. 2D cuts of the FPLEPS (top) and the CRP (bottom) PESs. The adsorbate sits in its equilibrium position and the *projectile* spans the (X, Z) plane for Y=a$\sqrt{2}$/8 (left) or the (Y, Z) plane for X = a/2 (right). Full lines (dashed lines) are positive (negative) isovalues separated by 0.2 eV.

2D-cuts of the 6D-potential energy in the ER entrance channel. The *target* atom is kept fixed in the atomic adsorption configuration (X_{ads}, Y_{ads}, Z_{ads}), whereas the *projectile* is allowed to move on two different planes: left (right) panels correspond to a 2D-cut for the *projectile* atom in the *X*,*Z* (*Y*,*Z*) plane characterized by $Y=Y_{ads}$ ($X=X_{ads}$). Negative values of the potential energy are indicated by dashed lines (the zero of the potential energy corresponding to the *target* in X_{ads}, Y_{ads}, Z_{ads} and the projectile located at the infinity of the surface). Figure 2 illustrates the large fraction of the configuration space energetically accessible for the *projectile*. In particular, in the (*Y*, *Z*)-plane characterized by $X = X_{ads}$ and for -1 Å $\leq Y \leq 0$, the *projectile* can reach *Z* values lower than the Z_{ads} allowing the *projectile* to *attack* the *target* from below. The two PESs are qualitatively very similar. However, close to the *target* position, some discrepancies are observed. For the 2D cuts of the PES considered in Fig. 2 we have found root mean square deviations (RMSD) of the FPLEPS and CRP PESs (with respect to a set of DFT data not used in the fitting/interpolation procedures) equal to 230 meV and 55 meV, respectively.

Figure 3 offers a comparison between both PESs and the Spin Polarized DFT (DFT-SP) data by showing 1D-cuts of the potential as a function of the *projectile* altitude for given impact parameters, b, along both *X* and *Y* directions. The *target* is fixed in the hollow site. For all impact parameters considered here, b = 0, 0.5, and 1.585 Å along *X* and *Y*, the agreement between DFT data and the CRP PES is very good (discrepancies being $\leq$ 0.1 eV). For small impact parameters, b = 0 and 0.5 Å, the FPLEPS is not as accurate as the CRP one. This could be due to the fact that FPLEPS model is, by construction, based on the fitting of DFT data corresponding to molecular dissociative adsorption channels and not specifically to ER entrance channel fitting. As a consequence, DFT data for vertical configurations ($\theta = 0$) around the hollow site were not included in the construction of the FPLEPS (see the Appendix for more details) following the prescription of the FPLEPS method exposed elsewhere.[54–56] For larger impact parameters, b = 1.585 Å, both the CRP and FPLEPS are in good agreement with the DFT data. Finally, as an additional evaluation of the accuracy of the FPLEPS and CRP PESs in regions of configuration space relevant for the dynamics, we have selected a set of $\sim$ 50 snapshots from 10 reactive trajectories in our QCT calculations (see Sec. III). Then, we evaluated the DFT-SP total energy of these configurations and we compared them with the values predicted by the FPLEPS and CRP PESs. The RMSD obtained in this way were 42 meV for the CRP and 142 meV for the FPLEPS. The FPLEPS fitting procedure is shown to be less accurate than the CRP interpolation scheme for reproducing the DFT calculations point to point, as already stated in early FPLEPS papers.[54–56] Our comparison of the ER dynamics for both PESs will allow us to explore the influence of the representation of the potential on the ER process.

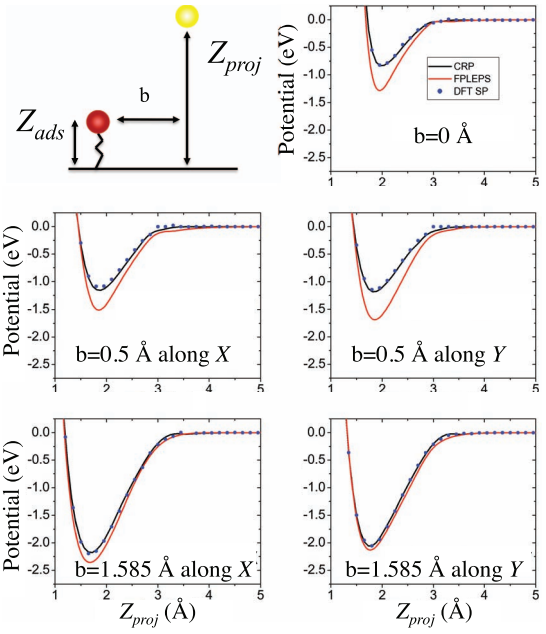

FIG. 3. Comparison between the CRP (black lines), the FPLEPS (red lines), and the DFT SP calculations (blue dots) in the ER entrance channel for impact parameters b = 0, 0.5, and 1.585 Å along *X* and *Y* directions.

III. DYNAMICS OF H_2 ELEY-RIDEAL RECOMBINATION ON W(110)

A. Methodology and computational details

We investigate normal incidence scattering dynamics of atomic hydrogen over H-pre-adsorbed W(110) surface within the Born Oppenheimer Static Surface approximation (BOSS) model via QCT. Neither electron-hole (e-h) pair excitations, nor energy dissipation to the surface phonons are taken into account. Electronic effects have been found negligible in the recombination of H_2 on Cu(111)[77] because of the ultrafast reaction time. Coupling to phonons are also expected to be small due to the large mass mismatch.[15,78]

The initial conditions for QCT simulations have been specified as follows: the *target*, located in the adsorption well, is given initial energies and random initial vibrational phases corresponding to the quasi-classical zero point energy (ZPE) of each normal mode, calculated within the harmonic approximation,.[18,20,26,36] Alternative Wigner distribution in the sampling of the *target* initial conditions have revealed very little differences from quasi-classical ZPE sampling for the ER recombination of H_2 on graphene.[36] The ZPE for vibrational motion normal to the surface is 71 meV (68 meV) for the CRP (FPLEPS). For parallel motion to the surface, the ZPE is 47 meV and 60 meV for the CRP respectively for the *X* and *Y* directions, and 55 meV for the FPLEPS on both directions. These values obtained with both PESs are in good agreement with theoretical[79,80] and experimental[81,82] values reported previously for H/W(110).

The initial altitude of the *projectile*, Z_{proj}, is chosen in the asymptotic region of the potential at 7.0 Å and perpendicular collision energies are sampled within the range 0.1–5.0 eV. Taking advantage of the symmetry of the H/W(110) unit cell, the initial coordinates (X_{proj},Y_{proj}) of the *projectile* are randomly sampled in the yellow area displayed in

Fig. 1(b). The ER cross section is thus defined by

$$\sigma_r = 2\int_D P_r(X_{proj}, Y_{proj})\, dX_{proj}\, dY_{proj}, \qquad (1)$$

D being the integration domain represented as the sampling area indicated in yellow on Fig. 1(b). $P_r(X_{proj}, Y_{proj})$, the two-dimensional opacity function, is the fraction of trajectories leading to an ER recombination for a given X_{proj} and Y_{proj} and averaged with respect to *target* initial coordinates and momenta. For each collision energy, 640 000 trajectories have been computed. ER recombination is considered to take place whenever both hydrogen atoms reach the initial altitude of the *projectile* with a positive H_2 center-of-mass momentum along Z, an inter-atomic distance $r \leq 2.2$ Å after only one rebound of the diatom center-of-mass along the trajectory.[83,84]

In order to compare our results with experimental data,[10] we have also performed QCT calculations using a generalized Langevin oscillator (GLO) model[85–89] to account for surface temperature effects and energy exchange with phonons.[83,84] However, we have found that adding such ingredients in the dynamics simulations barely alter the results obtained within the rigid surface approximation (at least, as far as the total ER reaction cross sections and products energy distributions are concerned).

B. Results and discussion

In Fig. 4, the ER recombination cross sections obtained with the FPLEPS and CRP PESs are presented as a function of the initial kinetic energy of the *projectile*, E_{proj}. The E_{proj}-dependence of both ER cross sections is very similar. First, they slightly increase with increasing E_{proj} up to 2 eV and then, decrease when E_{proj} increases. These cross sections remain low (maxima between 0.14 and 0.20 Å^2 for the FPLEPS and CRP PES, respectively), as already shown for H_2 recombination on metal surfaces (see, e.g., Refs. 14, 21, and 23). In the end, the differences between both PESs, discussed in Sec. II, seem to barely affect the dynamics.

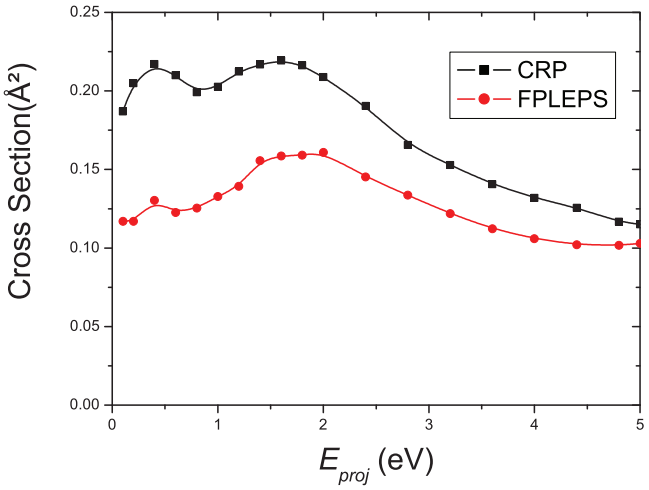

FIG. 4. Eley-Rideal recombination Cross Section, (Å^2), as a function of the initial kinetic energy of the *projectile*, E_{proj} (eV).

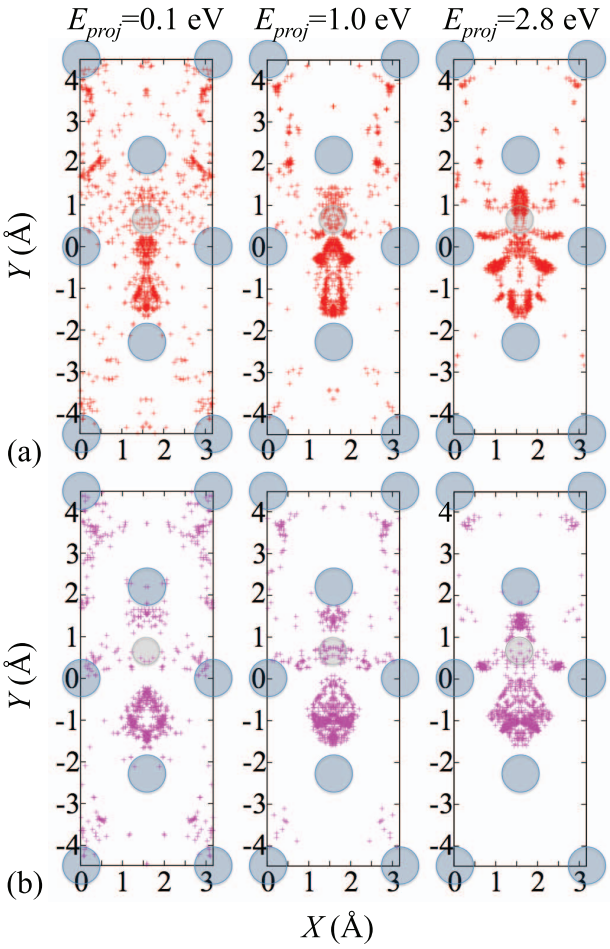

FIG. 5. Opacity maps obtained for dynamics simulations performed with the FPLEPS PES model: (a) (X, Y) initial positions of *projectiles* for trajectories leading to ER abstraction at three *projectile* energies (0.1, 1.0, and 2.8 eV), (b) (X, Y) rebound positions of *projectiles* for the same trajectories. For clarity only 1/5 of the trajectories have been represented.

For a better understanding of this result it is convenient to compare the opacity maps obtained with the FPLEPS and the CRP which are shown in Figs. 5 and 6 for three different values of E_{proj}: 0.1, 1.0, and 2.8 eV. In the upper panels, we represent the initial X, Y coordinates of the *projectile* for trajectories leading to ER recombination. In the lower panels, we show the X, Y coordinates of the points where the Z component of the *projectile* velocity changes from negative to positive (i.e., when the *projectile* rebounds).

The opacity maps obtained for both PES compare well: ER recombination is more likely to take place for similar initial positions of the *projectile*. Interestingly, only a minority of the reactive trajectories correspond to the *projectile* impinging on top of the initial position of the *target* atom in a collinear geometry. This clearly shows that the contribution of this particular initial condition to the ER total cross section is marginal. Moreover, the rebound position of the *projectile* for reactive trajectories starting near adsorption site are in general shifted away this site. Thus, the great majority of the ER abstraction events take place after a rebound of the *projectile* on a surface atom prior to recombination with the *target*. The main effect of this strong *projectile*/surface atom interaction is the redirection of the *projectile* towards the *target* favoring

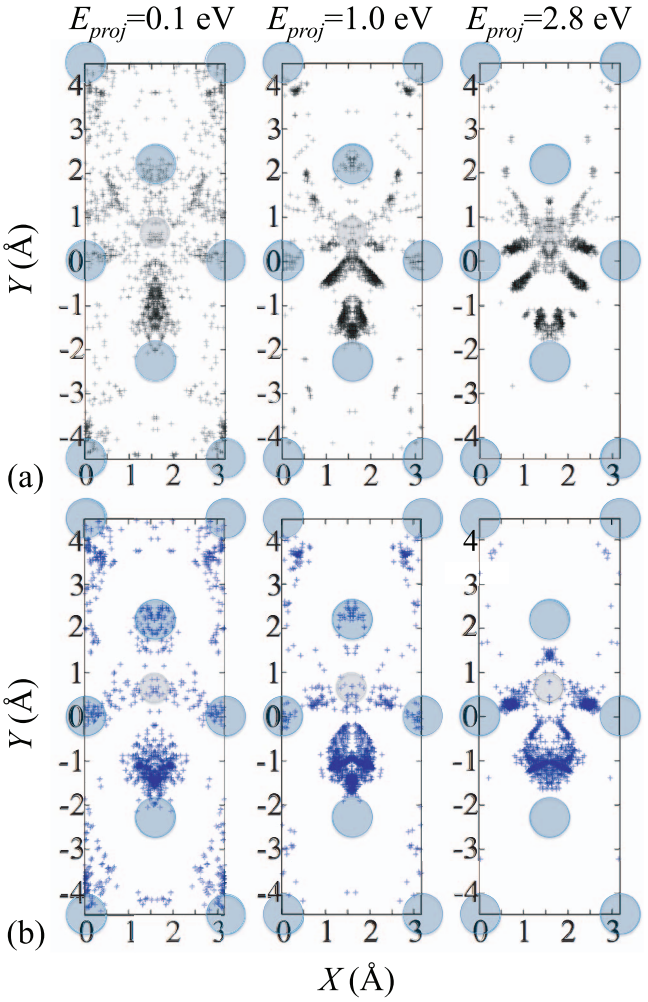

FIG. 6. Idem Fig. 5 but for dynamics simulations performed with the CRP PES.

the recombination and molecular abstraction in a rather direct process (after only one rebound of the *projectile*). Such a mechanism involving first a direct collision of the *projectile* with surface atoms explains why the rebound positions for reactive trajectories are focused near lines joining the *target* equilibrium position with its closest surrounding surface atoms.

As a result, opacity maps for rebound positions are in very good agreement when comparing the two PESs. However, dynamics on both PESs is not straightforwardly comparable trajectory per trajectory. Comparison is only meaningful by looking at groups of trajectories and under this consideration CRP and FPLEPS exhibit same dynamical behaviors.

An analysis of the *projectile* rebound position in *Z*, for reactive trajectories, is shown in Fig. 7 for the CRP PES case (at 0.1, 1.0, and 2.8 eV). The results for the FPLEPS PES (not shown) are very similar. As expected, the *Z* coordinate of the rebound position decreases when E_{proj} increases but even for the lowest energy considered (E_{proj} = 0.1 eV) most of the rebounds of the *projectile* take place below or around Z_{ads} ∼ 1.1 Å. These results indicate that most ER recombination events take place for the *projectile attacking* the *target* from below or from the side after a first collision with one of the surface atoms closest to the *target*.

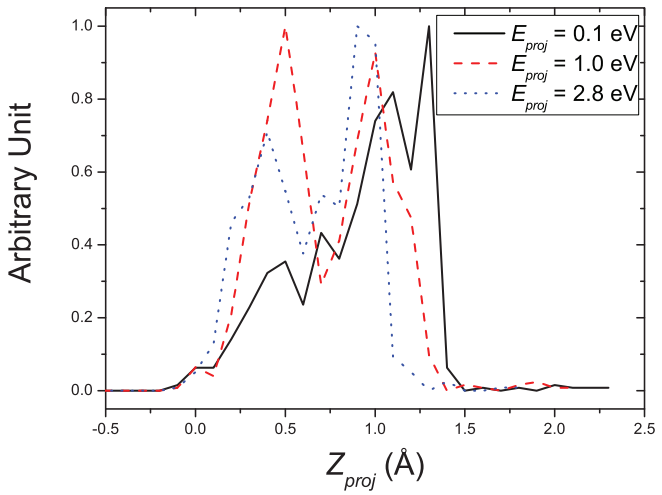

FIG. 7. Distribution of the *Z* coordinate of the rebound position vector of the *projectile* obtained in the QCT calculations using the CRP PES.

In Fig. 8, the mean final translational energy, together with mean rotational and vibrational energies of the recombined H_2 molecules are displayed as a function of E_{proj}. Rotationally and vibrationally excited products are observed, as expected for a process whose exothermicity is ∼1.8 eV. Such rovibrational excitations increase when the initial kinetic energy of the *projectile* increases. Nevertheless, the major part of the energy remains in translational motion. Such results compare well with studies of H_2 recombination on other metal surfaces.[14,19] Dynamical observables reveal a semi-quantitative agreement for both CRP-PESs and FPLEPS (lower than 20% relative differences), thus suggesting that the dynamics bears similarities, regardless the discrepancies highlighted above.

The vibrational state distribution of H_2 molecules recombining on a polycrystalline W sample, which were measured by Markelj *et al.*,[10] are displayed in Fig. 9. Experimentally, atom recombination was observed in a cell where a tungsten sample was exposed to hydrogen atoms resulting from hydrogen molecules dissociation on a hot tungsten filament. The atomic gas temperature was estimated to be ∼2000 K whereas the tungsten surface sample temperature was maintained to ∼300 K. Vibrationally highly excited hydrogen molecules (up to v = 9) were observed. Such strong excitations were attributed to ER recombination with H atoms adsorbed in low energy binding sites of the polycrystalline tungsten surface. Such results gave comparable results with former experiments.[6–8] However it is worth mentioning that the population of excited levels higher than v = 3 is very small ($<1.5\ 10^{-3}$).

To compare with experiments, vibrational state distributions have been computed by thermal averaging normal collision energy resolved results in the limit of normal and total energy scaling.[90] Both limits give almost identical results as vibrational state distributions depend weakly on collision energy, in particular for E_{proj} > 0.1 eV leading to non-negligible cross-sections. Hereafter, we only consider the normal energy scaling limit. As apparent from Fig. 9, QCT results, computed within the standard binning method,[91] are in

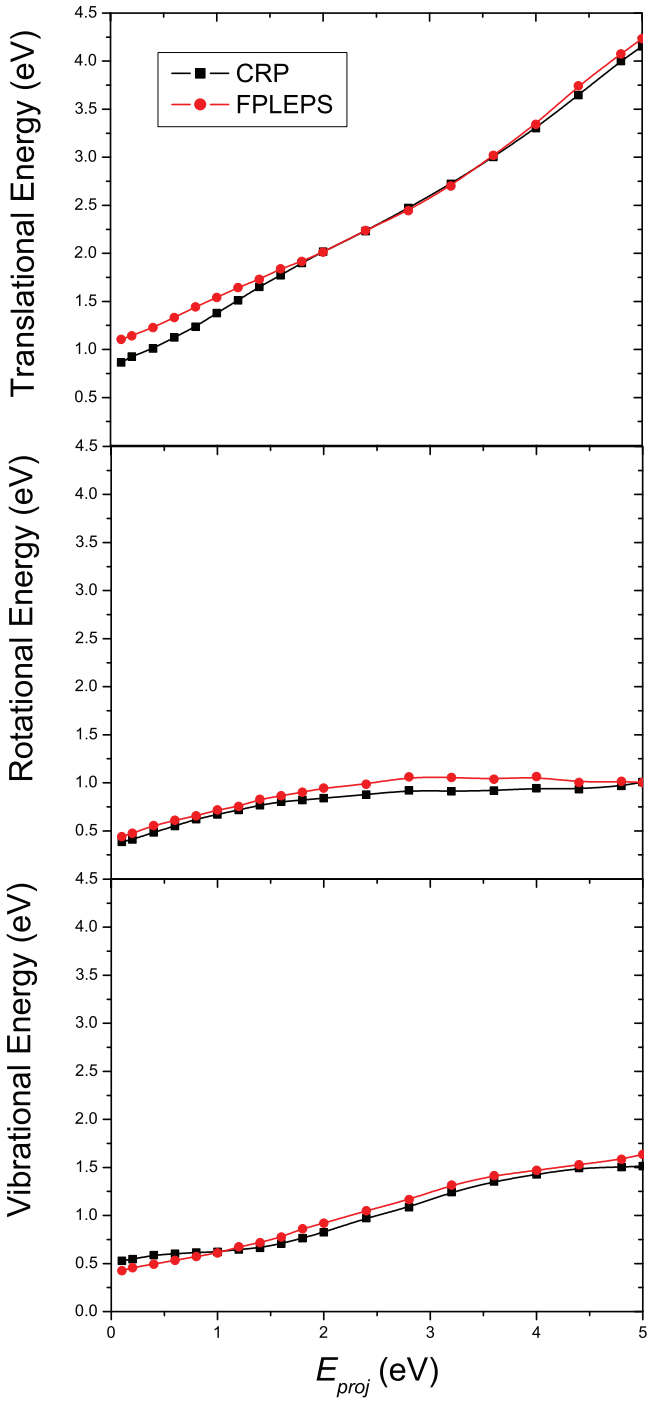

FIG. 8. Final translational (upper panel), rotational (middle), and vibrational (lower panel) final energies of the H_2 recombined molecules as a function of E_{proj}.

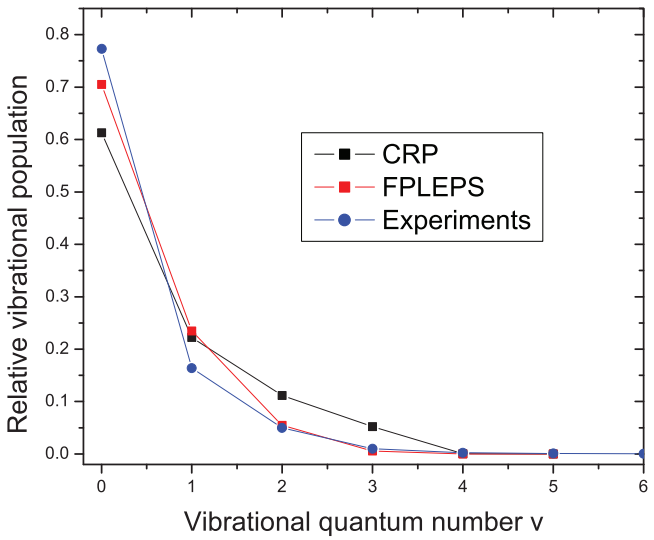

FIG. 9. Relative vibrational populations of the produced molecules. Results for the Extended-CRP are in black squares and for the FPLEPS in red squares whereas experiments results[10] are in blue dots. Lines are drawn to guide the eye. For clarity of the figure, experimental results for excitations higher than v = 6 are not represented.

remarkable agreement with experiments up to v = 5 vibrational state for the FPLEPS PES. The choice of the binning procedure for vibrational action[92,93] has negligible influence on vibrational state distribution. In view of the simplifications of the present theoretical treatment, such a good agreement might result from a cancellation of error. The experiments use polycrystalline W samples (including defects) and might be sensitive to "Hot Atom" (HA) processes whereas our simulations are restricted to ultrafast abstraction in the zero coverage limit off a perfect W(110) surface. However, these results might suggest the vibrational distribution of H_2 molecule resulting from ER abstraction is weakly sensitive to surface symmetry. Additional studies for H+H/W(100) are currently underway to address the role of surface symmetry as well as isotope effects. The CRP PES leads to a somewhat hotter vibrational distribution, but with comparable trend. For both PESs, the ER process leads to molecules vibrationally hotter than the gas in contact with the W sample (∼2000 K), because 20%-30% of the total initial energy is driven into vibration. Interestingly, the population of the lowest 4 vibrational levels are in reasonable agreement with experiments. In any case, the comparison with experiments must be made with caution because additional ingredients not considered in the present dynamics simulations might be necessary: e.g., abstraction from other faces of W in the polycrystalline sample, H-coverage effects, and the role of HA.

In this perspective, the apparent better agreement of the FPLEPS with experiments does not allow to conclude on a better performance of this PES representation.

Besides, our results are hardly comparable with previous works.[11,37,94] Indeed, in such previous works, because of the little rotational excitation experimentally observed in earlier experiments,[6] ER cross section was assumed to proceed via collinear vertical collision between both H atoms. In the present 6D calculations, the collinear case, as for most of H+H/metal systems with high binding energies,[13,14,23] contributes to less than 5% of the recombination cross section and rotational excitation is as high as vibrational one. As in other systems,[83,84] ER recombination is found to mainly occur via collision with surface atoms prior to recombination underlying the fact that the representation of the PES has to be accurate more specifically in ER entrance channels corresponding to large impact parameters where both PES are in really good agreement to DFT energies (see Fig. 3 at b = 1.585 Å).

IV. CONCLUSION

The Eley-Rideal (ER) abstraction dynamics of H_2 on W(110) has been analyzed through Quasi Classical Trajectory (QCT) calculations. We have used two potential energy surfaces (PESs) obtained with different parametrization methods based on Density Functional Theory (DFT) data: the interpolation corrugation reducing procedure (CRP), and the fitting to a Flexible Periodic London-Eyring-Polanyi-Sato (FPLEPS) functional form. The obtained ER cross sections, final translational, rotational, and vibrational energies of the formed molecules are similar in spite of some sizable discrepancies between both PESs, in particular for small impact parameters of the projectile. In contrast with the usual belief, the PES features corresponding to quasi-collinear impact geometry has a minor influence on the ER dynamics. Collisions with large impact parameters (for which both PESs are more accurate and agree with each other) contribute more to the ER process which is most likely to take place after a rebound of the projectile against a surface atom allowing an attack from the back on the target atom. Finally, also important is the role played by the reaction exothermicity (being equally well represented by the two PESs used) which determines in great extent the final energy of the nascent molecules.

ACKNOWLEDGMENTS

The authors acknowledge ECOS-sud program for funding and Mesocentre de Calcul Intensif Aquitain (MCIA) for computer resources. A.E.M. and H.F.B. also acknowledge financial support from CONICET (project PIP 0667), ANPCyT (project PICT Bicentenario No. 1962), and UNR (project PID ING404).

APPENDIX: PES MODEL

1. DFT calculations

The FPLEPS and the CRP PESs, which are presented in Subsections 2 and 3 of the Appendix, rely on the DFT calculations performed using parameters detailed by Busnengo *et al.* in the study of dissociative adsorption of H_2 on W(100) and W(110).[42] They were carried out with the Vienna *Ab initio* Simulation Package (VASP)[95–99] within the slab supercell approach and using the generalized gradient approximation (GGA) proposed by Perdew and Wang (PW91) for the exchange-correlation functional.[100] Plane wave basis set is used for the description of electronic wave functions with a cut-off energy of 230 eV. Interactions with the atomic cores is described by ultrasoft pseudopotentials (US).[101] A five layers W slab for which the inter layer distances have been optimized was employed to represent a (2×2) cell with 15 Å vacuum space between consecutive slabs. The *k*-point sampling of the Brillouin zone made use of a Monkhorst-Pack (5×5×1) grid and an electron smearing of $\sigma = 0.4$ eV was introduced. To extend the CRP PES of Ref. 42, both non-spin polarized (NSP) and spin polarized (SP) DFT calculations were required. Indeed, the description of the ER entrance channel (the *target* atom adsorbed in its equilibrium position and the *projectile* atom approaching from the gas phase) requires taking into account the spin magnetization of the impinging H atom. The initial magnetization of the H *projectile* atom results equal to 1 μ_B far from the surface and gradually falls down to 0 μ_B when the atom gets close to the surface.

2. The FPLEPS PES

The FPLEPS analytical functional form[54–56] was recently developed to extend the validity of the periodic LEPS[7,44,101–105] to the description of strongly corrugated diatom-surface interactions. The six-dimensional potential $V^{6D}(\mathbf{r}_{\mathbf{H_A}}, \mathbf{r}_{\mathbf{H_B}})$ of the two H atoms over an infinite and periodic surface is expressed as a function of the two coordinate vectors $\mathbf{r}_{\mathbf{H_A}}(X_A, Y_A, Z_A)$ and $\mathbf{r}_{\mathbf{H_B}}(X_B, Y_B, Z_B)$ (see Fig. 1) in a coordinate system with the origin on a topmost layer surface atom:

$$\begin{aligned} V^{6D}(\mathbf{r}_{\mathbf{H_A}}, \mathbf{r}_{\mathbf{H_B}}) = {} & U_{H_AW}(\mathbf{r}_{\mathbf{H_A}}) + U_{H_BW}(\mathbf{r}_{\mathbf{H_B}}) \\ & + U_{H_2}(\|\mathbf{r}_{\mathbf{H_A}} - \mathbf{r}_{\mathbf{H_B}}\|) \\ & - \left(Q^2_{H_2}(\|\mathbf{r}_{\mathbf{H_A}} - \mathbf{r}_{\mathbf{H_B}}\|)\right. \\ & + \left(Q_{H_AW}(\mathbf{r}_{\mathbf{H_A}}) + Q_{H_BW}(\mathbf{r}_{\mathbf{H_B}})\right)^2 \\ & - Q_{H_2}(\|\mathbf{r}_{\mathbf{H_A}} - \mathbf{r}_{\mathbf{H_B}}\|)\left(Q_{H_AW}(\mathbf{r}_{\mathbf{H_A}})\right. \\ & \left.\left. + Q_{H_BW}(\mathbf{r}_{\mathbf{H_B}})\right)\right)^{\frac{1}{2}} \\ & + A_g \exp\left[-\frac{(Z_{CM} - Z_g^0)^2}{\sigma_g^2}\right], \end{aligned} \tag{A1}$$

where U_i and Q_i are the Coulomb and exchange integrals for the two body terms respectively (i stands for H_2, H_AW, and H_BW). Z_{CM} is the altitude of the center of mass (CM) of the molecule. A_g, Z_g^0, and σ_g are the parameters of a Gaussian function which has been originally introduced to correctly fit multiple barrier structures appearing in 2D-(Z_{CM}, r) DFT cuts describing dissociative adsorption. A_g is the amplitude, Z_g^0 and σ_g, respectively the position of the maximum/minimum and a parameter controlling the width of the Gaussian function. When the bonding and anti-bonding states of the two body terms are approximated with Morse and anti-Morse functions, U_i and Q_i read:

$$\begin{aligned} U_i = \frac{D_i}{4(1+\Delta_i)}\big[&(3+\Delta_i)\exp\left(-2\alpha_i(d_i - d_i^{eq})\right) \\ &-(2+6\Delta_i)\exp\left(-\alpha_i(d_i - d_i^{eq})\right)\big] \end{aligned} \tag{A2}$$

$$\begin{aligned} Q_i = \frac{D_i}{4(1+\Delta_i)}\big[&(1+3\Delta_i)\exp\left(-2\alpha_i(d_i - d_i^{eq})\right) \\ &-(6+2\Delta_i)\exp\left(-\alpha_i(d_i - d_i^{eq})\right)\big] \end{aligned} \tag{A3}$$

with $d_i = \|\mathbf{r}_{\mathbf{H_B}} - \mathbf{r}_{\mathbf{H_A}}\|$ for $i = H_2$ and $d_i = Z_A$ (Z_B) for $i = H_AW$ (H_BW). D_i, α_i, and d_i^{eq} are the Morse parameters, determined by least square fitting of DFT points. For H_AW and H_BW interactions, such parameters are expanded in Fourier series adapted to the (110) symmetry of the bcc crystal. The Sato parameters, Δ_{H_AW} (=Δ_{H_BW}) and Δ_{H_2} describe the strong interaction region of the PES. The Gaussian

function and Sato parameters depend not only on the orientation of the molecule with respect to the surface, defined by the two angles θ and ϕ (see Fig. 1) but also on the lateral position of the CM of the molecule (X_{CM}, Y_{CM}). Such parameters are computed by a least-square fitting of the two-dimensional 2D-(Z_{CM}, r) DFT cuts, where r is the interatomic distance ($r = \|\mathbf{r}_{\mathbf{H_A}} - \mathbf{r}_{\mathbf{H_B}}\|$), on high symmetry sites. The angular interpolation over (θ, ϕ) is performed using a symmetry adapted expansion of trigonometric functions and a Fourier series is employed to describe the (X, Y) dependence of the molecular parameters (Gaussian an Sato parameters). The molecular parameters were fitted on 2D-(Z_{CM}, r) DFT cuts computed by Busnengo *et al.*[42] The details for the implementation of the FPLEPS can be found in Ref. 56. The FPLEPS is thus not specifically fitted in the ER entrance channel but is asymptotically correct by construction.

The original building procedure of the FPLEPS has been followed so the Sato and Gaussian parameters are fitted on high symmetry sites.[54–56]

3. The CRP PES

The CRP relies on the fact that most of the strong corrugation of the molecule-surface PESs is due to the atom-surface interaction. Therefore, it is convenient to decompose the full 6D PES as the sum of the atom-surface potentials and a remaining six-dimensional function usually called 6D interpolation function. In the case of H_2/W(110), the 6D PES can be written as:

$$\begin{aligned} V_{H_2/W(110)}(X_{CM}, Y_{CM}, Z_{CM}, r, \theta, \phi) &= I_{H_2/W(110)}(X_{CM}, Y_{CM}, Z_{CM}, r, \theta, \phi) \\ &+ V_{H/W(110)}(X_A, Y_A, Z_A) \\ &+ V_{H/W(110)}(X_B, Y_B, Z_B), \end{aligned} \tag{A4}$$

where $V_{H/W(110)}$ is the atom-surface potential, and $I_{H_2/W(110)}$ is the interpolation function. The use of Eq. (A4) allows one to interpolate $I_{H_2/W(110)}$ and $V_{H/W(110)}$ instead of the full potential. On the one hand, the interpolation of the atom-surface potential is relatively simple because of its 3D character, and on the other hand, $I_{H_2/W(110))}$ is a much smoother function of X_{CM}, Y_{CM},θ, and ϕ than the full potential. Thus, even a relatively small number 2D cuts-(Z_{CM}, r) allow an accurate interpolation of the interpolation function over the remaining four molecular coordinates (see Refs. 60 and 62 for a full description of the CRP method).

Though the corrugation reducing strategy is valid throughout the six-dimensional molecule-surface configuration space and so, suitable to investigate any reactive or unreactive molecule-surface process, the CRP method has been mostly applied to study dissociative adsorption. In the case of singlet-ground-state molecules (e.g., H_2 and N_2) on non-magnetic surfaces, dissociative adsorption takes place entirely in a region of configuration space where NSP calculations provide a reliable description of the molecule-surface PES. Thus, for H_2/W(110) the CRP PESs of Ref. 42 was built from NSP DFT results only. However, as mentioned above, the entrance channel of Eley-Rideal reactions is characterized by the presence of a single atom far from the surface which requires SP DFT calculations.[44] In the particular case of H_2 interacting with W(110) (and other non-magnetic metal surfaces[44]), SP DFT calculations are required whenever the interatomic distance $r \gtrsim 1.6$ Å and at least one of the atoms is relatively far from the surface, e.g., for $Z \gtrsim 2.6$ Å. Therefore, we have carried out extra SP DFT atom-surface calculations for $Z > 2.6$ Å and molecule-surface calculations for 1.6 Å $\leq r \leq 3$ Å.

In the case of the SP atom-surface potential, $V^{SP}_{H/W(110)}$, we have carried out a direct interpolation (using 3D cubic splines) of the SP data because for $Z > 2.6$ Å the atom-surface PES corrugation is relatively weak. Then, an asymptotically correct atom-surface potential for H/W(110), $V_{H/W(110)}$, was obtained as follows:

$$\begin{aligned} V_{H/W(110)}(X, Y, Z) = V^{NSP}_{H/W(110)}(X, Y, Z) f_{\alpha,\beta}(Z) \\ + V^{SP}_{H/W(110)}(X, Y, Z)[1 - f_{\alpha,\beta}(Z)], \end{aligned} \tag{A5}$$

where $V^{NSP}_{H/W(110)}$ is the NSP atom-surface PES of Ref. 42 and $f_{\alpha,\beta}(Z)$ a smooth switch off function equal to 1 (0) for $Z \leq \alpha$ ($Z \geq \beta$).

The SP molecule-surface DFT data were interpolated also using the CRP and assuming that for $r > 1.6$ Å, $I_{H_2/W(110)}$ only depends on r,Z_{CM},θ. This is justified by the fact that for large r values, $I_{H_2/W(110)}$ becomes less dependent on the lateral position and azimuthal orientation of the H_2 molecule and approaches to zero (see Eq. (A4)). Thus, we have only carried out SP DFT calculations on the long bridge site (Fig. 1) for the perpendicular ($\theta = 0$) and a parallel ($\theta = \pi/2$,$\phi = \pi/2$) configuration. Then, the molecule-surface SP interpolation function, $I^{SP}_{H_2/W(110)}$, was written as:

$$I^{SP}_{H_2/W(110)}(r, Z_{CM}, \theta) = \left[\frac{A(r, Z_{CM})}{2} + \frac{B(r, Z_{CM})}{2}\cos(2\theta)\right] f_{\gamma,\delta}(r) \tag{A6}$$

being

$$\begin{aligned} A(r, Z_{CM}) &= V^{SP}(\theta = 0) + V^{SP}(\theta = \pi/2, \phi = \pi/2) \\ B(r, Z_{CM}) &= V^{SP}(\theta = 0) - V^{SP}(\theta = \pi/2, \phi = \pi/2), \end{aligned} \tag{A7}$$

$\gamma = 2.75$ Å, and $\delta = 3.0$ Å. Thus, for $r \geq 3$ Å the SP PES is simply the sum of the two atom-surface potentials (Eq. (A5)). The full SP molecule-surface PES can be computed using Eq. (A4). It is worth to emphasize that in spite of the 3D character of $I^{SP}_{H_2/W(110)}$, the corresponding SP PES obtained for $r \geq 1.6$ Å is six dimensional due to the presence of the atom-surface potentials. Finally, the 6D PES of $H_2/W(110)$ was approximated by

$$\begin{aligned} V_{H_2/W(110)}(X_{CM}, Y_{CM}, Z_{CM}, r, \theta, \phi) &= V^{NSP}_{H_2/W(110)}(X_{CM}, Y_{CM}, Z_{CM}, r, \theta, \phi) f_{\chi,\rho}(r) \\ &+ V^{SP}_{H_2/W(110)}(X_{CM}, Y_{CM}, Z_{CM}, r, \theta, \phi)[1 - f_{\chi,\rho}(r)] \end{aligned} \tag{A8}$$

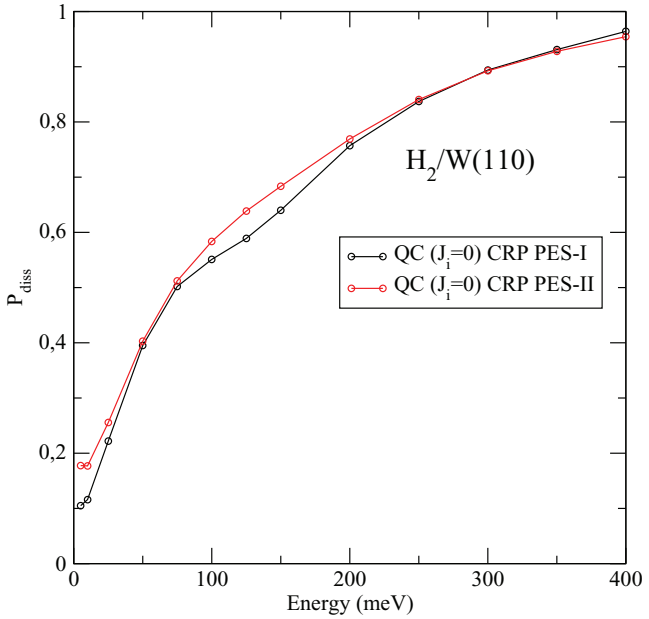

FIG. 10. Comparison of the H_2 dissociative adsorption probabilities as a function of impact energy, E_i, at normal incidence obtained with the 6D PES of Ref. 42 (PES-I) and the one presented in the present work (PES-II).

with $\chi = 1.55$ Å and $\rho = 1.75$ Å. In Eq. (9), $V^{NSP}_{H_2/W(110)}$ is a NSP molecule-surface PES similar to the one described in Ref. 42. The only difference between $V^{NSP}_{H_2/W(110)}$ and that of Ref. 42 is that, in order to improve the description of the energy of molecular configurations in the entrance channel of the ER reaction, we have added DFT data for molecular configurations on three additional surface sites: (X_{CM}, Y_{CM}) = (a/4, a$\sqrt{2}$/8), (a/2, a$\sqrt{2}$/8), and (a/2, 3a$\sqrt{2}$/8) (for $\theta = 0$, $\pi/4$, and π) as well as new configurations with $\theta = \pi/4$ on the high symmetry sites top and long bridge (Fig. 1). Thus, $V_{H_2/W(110)}$ (hereafter referred to as PES-II) is based on 56 molecular configurations (X_{CM}, Y_{CM}, θ, ϕ) whereas the 6D PES of Ref. 42 (hereafter referred to as PES-I) was based on only 26 molecular configurations. Interestingly, the dissociative adsorption probabilities obtained with both PESs are quite similar (Fig. 10) in spite of the large number of additional data used in the new PES presented in the present work.

[1]A. W. Kleyn, N. J. L. Cardozo, and U. Samm, Phys. Chem. Chem. Phys. **8**, 1761 (2006).
[2]V. Barabash, G. Federici, R. Matera, A. R. Raffray, and I. H. Teams, Phys. Scr. **T81**, 74 (1999).
[3]M. H. J. 't Hoen, M. Mayer, A. W. Kleyn, and P. A. Zeijlmans van Emmichoven, Phys. Rev. Lett. **111**, 225001 (2013).
[4]D. Eley and E. Rideal, Nature (London) **146**, 401 (1940).
[5]W. H. Weinberg, in *Dynamics of Gas Surface Interactions*, edited by C. T. Rettner and M. N. R. Ashfold (Royal Society of Chemistry, London, 1991), Chap. 5, pp. 171–219.
[6]R. I. Hall, I. Cadez, M. Landau, F. Pichou, and C. Schermann, Phys. Rev. Lett. **60**, 337 (1988).
[7]P. J. Eenshuistra, J. H. M. Bonnie, J. Los, and H. J. Hopman, Phys. Rev. Lett. **60**, 341 (1988).
[8]C. Schermann, F. Pichou, M. Landau, I. Cadez, and R. I. Hall, J. Chem. Phys. **101**, 8152 (1994).
[9]P. Vankan, D. Schram, and R. Engeln, Chem. Phys. Lett. **400**, 196 (2004).
[10]S. Markelj and I. Cadez, J. Chem. Phys. **134**, 124707 (2011).
[11]B. Jackson and M. Persson, J. Chem. Phys. **96**, 2378 (1992).
[12]M. Persson and B. Jackson, J. Chem. Phys. **102**, 1078 (1995).
[13]B. Jackson and M. Persson, J. Chem. Phys. **103**, 6257 (1995).
[14]S. Caratzoulas, B. Jackson, and M. Persson, J. Chem. Phys. **107**, 6420 (1997).
[15]D. V. Shalashilin and B. Jackson, J. Chem. Phys. **109**, 2856 (1998).
[16]D. V. Shalashilin, B. Jackson, and M. Persson, Faraday Discuss. **110**, 287 (1998).
[17]C. Kalyanaraman, D. Lemoine, and B. Jackson, Phys. Chem. Chem. Phys. **1**, 1351 (1999).
[18]D. V. Shalashilin, B. Jackson, and M. Persson, J. Chem. Phys. **110**, 11038 (1999).
[19]B. Jackson and D. Lemoine, J. Chem. Phys. **114**, 474 (2001).
[20]Z. B. Guvenc, X. Sha, and B. Jackson, J. Chem. Phys. **115**, 9018 (2001).
[21]Z. B. Guvenc, X. Sha, and B. Jackson, J. Phys. Chem. B **106**, 8342 (2002).
[22]Z. B. Guvenc and D. Guvenc, Surf. Sci. **529**, 11 (2003).
[23]R. Martinazzo, S. Assoni, G. Marinoni, and G. F. Tantardini, J. Chem. Phys. **120**, 8761 (2004).
[24]G. Lanzani, R. Martinazzo, G. Materzanini, I. Pino, and G. F. Tantardini, Theor. Chem. Acc. **117**, 805 (2007).
[25]D. Lemoine, J. D. Quattrucci, and B. Jackson, Phys. Rev. Lett. **89**, 268302 (2002).
[26]J. G. Quattrucci, B. Jackson, and D. Lemoine, J. Chem. Phys. **118**, 2357 (2003).
[27]M. Persson and B. Jackson, Chem. Phys. Lett. **237**, 468 (1995).
[28]S. Morisset, A. Aguillon, M. Sizun, and V. Sidis, Chem. Phys. Lett. **378**, 615 (2003).
[29]S. Morisset, A. Aguillon, M. Sizun, and V. Sidis, J. Chem. Phys. **121**, 6493 (2004).
[30]S. Morisset, A. Aguillon, M. Sizun, and V. Sidis, J. Phys. Chem. A **108**, 8571 (2004).
[31]S. Morisset and A. Allouche, J. Chem. Phys. **129**, 024509 (2008).
[32]S. Morisset, Y. Ferro, and A. Allouche, Chem. Phys. Lett. **477**, 225 (2009).
[33]S. Morisset, Y. Ferro, and A. Allouche, J. Chem. Phys. **133**, 044508 (2010).
[34]S. Cazaux, S. Morisset, M. Spaans, and A. Allouche, Astron. Astrophys. **535**, A27 (2011).
[35]D. Bachellerie, M. Sizun, A. Aguillon, D. Teillet-Billy, N. Rougueau, and V. Sidis, Phys. Chem. Chem. Phys. **11**, 2715 (2009).
[36]M. Sizun, D. Bachellerie, A. Aguillon, and V. Sidis, Chem. Phys. Lett. **498**, 32 (2010).
[37]P. Kratzer and W. Brenig, Surf. Sci. **254**, 275 (1991).
[38]M. Rutigliano and M. Cacciatore, Phys. Chem. Chem. Phys. **13**, 7475 (2011).
[39]A. Forni, M. C. Desjonquères, D. Spanjaard, and G. F. Tantardini, Surf. Sci. **274**, 161 (1992).
[40]A. Forni, M. C. Desjonquères, D. Spanjaard, and G. F. Tantardini, Surf. Sci. **269–270**, 201 (1992).
[41]M. Barnes and R. Willis, Phys. Rev. Lett. **41**, 1729 (1978).
[42]H. F. Busnengo and A. E. Martinez, J. Phys. Chem. C **112**, 5579 (2008).
[43]B. Jackson, M. Persson, and B. D. Kay, J. Chem. Phys. **100**, 7687 (1994).
[44]M. Persson, J. Stroemquist, L. Bengtsson, B. Jackson, D. V. Shalashilin, and B. Hammer, J. Chem. Phys. **110**, 2240 (1999).
[45]B. Jackson in *The Chemical Physics of Solid Surfaces*, edited by D. Woodruff (Elsevier, Amsterdam, 2003), Vol. 11, pp. 51–77.
[46]J. G. Quattrucci and B. Jackson, J. Chem. Phys. **122**, 074705 (2005).
[47]A. Groß and A. Dianat, Phys. Rev. Lett. **98**, 206107 (2007).
[48]A. Groß, Phys. Rev. Lett. **103**, 246101 (2009).
[49]A. Lozano, A. Gross, and H. F. Busnengo, Phys. Chem. Chem. Phys. **11**, 5814 (2009).
[50]M. Blanco-Rey, J. Juaristi, R. D. Muiño, H. Busnengo, G. Kroes, and M. Alducin, Phys. Rev. Lett. **112**, 103203 (2014).
[51]S. Casolo, G. F. Tantardini, and R. Martinazzo, Proc. Natl. Acad. Sci. **110**, 6674 (2013).
[52]A. Fernández-Ramos, J. A. Miller, S. J. Klippenstein, and D. G. Truhlar, Chem. Rev. **106**, 4518 (2006).
[53]P. Gamallo, L. Martin-Gondre, R. Sayós, C. Crespos, and P. Larrégaray, in *Dynamics of Gas Surface Interactions*, Springer Series in Surface Sciences Vol. 50, edited by R. Díez-Muiño and H. F. Busnengo (Springer, 2013), Chap. 2, pp. 25–50.
[54]L. Martin-Gondre, C. Crespos, P. Larrégaray, J.-C. Rayez, B. van Ootegem, and D. Conte, Chem. Phys. Lett. **471**, 136 (2009).
[55]L. Martin-Gondre, C. Crespos, P. Larrégaray, J.-C. Rayez, D. Conte, and B. van Ootegem, Chem. Phys. **367**, 136 (2010).
[56]L. Martin-Gondre, C. Crespos, P. Larrégaray, J.-C. Rayez, B. van Ootegem, and D. Conte, J. Chem. Phys. **132**, 204501 (2010).

[57]F. London, Z. Elektrochem **35**, 552 (1929).
[58]H. Eyring and M. Polanyi, Z. Phys. Chem. **12**, 279 (1931).
[59]P. J. Kuntz, E. M. Nemeth, J. C. Polanyi, S. D. Rosner, and C. E. Young, J. Chem. Phys. **44**, 1168 (1966).
[60]H. F. Busnengo, A. Salin, and W. Dong, J. Chem. Phys. **112**, 7641 (2000).
[61]G. Kresse, Phys. Rev. B **62**, 8295 (2000).
[62]R. A. Olsen, H. F. Busnengo, A. Salin, M. F. Somers, G. J. Kroes, and E. J. Baerends, J. Chem. Phys. **116**, 3841 (2002).
[63]C. Diaz, R. A. Olsen, H. F. Busnengo, and G. J. Kroes, J. Phys. Chem. C **114**, 11192 (2010).
[64]A. Salin, J. Chem. Phys. **124**, 104704 (2006).
[65]H. F. Busnengo, W. Dong, and A. Salin, Chem. Phys. Lett. **320**, 328 (2000).
[66]H. F. Busnengo, C. Crespos, W. Dong, J. C. Rayez, and A. Salin, J. Chem. Phys. **116**, 9005 (2002).
[67]E. Pijper, M. F. Somers, G. J. Kroes, R. A. Olsen, E. J. Baerends, H. F. Busnengo, A. Salin, and D. Lemoine, Chem. Phys. Lett. **347**, 277 (2001).
[68]G. Volpilhac and A. Salin, Surf. Sci. **556**, 129 (2004).
[69]M. Luppi, D. A. McCormack, R. A. Olsen, and E. J. Baerends, J. Chem. Phys. **123**, 164702 (2005).
[70]M. Luppi, R. A. Olsen, and E. J. Baerends, Phys. Chem. Chem. Phys. **8**, 688 (2006).
[71]M. Alducin, R. Díez-Muiño, H. F. Busnengo, and A. Salin, Phys. Rev. Lett. **97**, 056102 (2006).
[72]M. Alducin, R. Díez-Muiño, H. F. Busnengo, and A. Salin, J. Chem. Phys. **125**, 144705 (2006).
[73]G. Bocan, R. Díez, M. Alducin, and H. F. Busnengo, J. Chem. Phys. **128**, 154704 (2008).
[74]M. Alducin, H. F. Busnengo, and R. Díez-Muiño, J. Chem. Phys. **129**, 224702 (2008).
[75]F. Nattino, C. Díaz, B. Jackson, and G.-J. Kores, Phys. Rev. Lett. **108**, 236104 (2012).
[76]A. Perrier, L. Bonnet, D. A. Liotard, and J. C. Rayez, Surf. Sci. **581**, 189 (2005).
[77]H. Nienhaus, Surf. Sci. Rep. **45**, 1 (2002).
[78]J. Strömquist, L. Bengtsson, M. Persson, and B. Hammer, Surf. Sci. **397**, 382 (1998).
[79]A. Nojima and K. Yamashita, Surf. Sci. **601**, 3003 (2007).
[80]P. Nordlander, S. Holloway, and J. Norskov, Surf. Sci. **136**, 59 (1984).
[81]M. Balden, S. Lehwald, H. Ibach, and D. L. Mills, Phys. Rev. Lett. **73**, 854 (1994).
[82]M. Balden, S. Lehwald, and H. Ibach, Phys. Rev. B **53**, 7479 (1996).
[83]E. Quintas-Sánchez, P. Larrégaray, C. Crespos, L. Martin-Gondre, J. Rubayo-Soneira, and J.-C. Rayez, J. Chem. Phys. **137**, 064709 (2012).
[84]E. Quintas-Sánchez, C. Crespos, J.-C. Rayez, L. Martin-Gondre, and J. Rubayo-Soneira, J. Chem. Phys. **138**, 024706 (2013).
[85]S. A. Adelman, J. Chem. Phys. **71**, 4471 (1979).
[86]J. C. Tully, J. Chem. Phys. **73**, 1975 (1980).
[87]M. Dohle, P. Saalfrank, and T. Uzer, J. Chem. Phys. **108**, 4226 (1998).
[88]J. C. Polanyi and R. J. Wolf, J. Chem. Phys. **82**, 1555 (1985).
[89]H. F. Busnengo, W. Dong, and A. Salin, Phys. Rev. Lett. **93**, 236103 (2004).
[90]M. Ramos, M. Minniti, C. Díaz, R. Miranda, F. Martin, A. E. Martinez, and H. F. Busnengo, Phys. Chem. Chem. Phys. **15**, 14936 (2013).
[91]K. S. Bradley and G. C. Schatz, J. Phys. Chem. **98**, 3788 (1994).
[92]L. Bonnet and J. C. Rayez, Chem. Phys. Lett. **277**, 183 (1997).
[93]L. Bonnet and J. C. Rayez, Chem. Phys. Lett. **397**, 106 (2004).
[94]B. Jackson and M. Persson, Surf. Sci. **269–270**, 195 (1992).
[95]G. Kresse and J. Hafner, Phys. Rev. B **47**, 558 (1993).
[96]G. Kresse and J. Hafner, Phys. Rev. B **48**, 13115 (1993).
[97]G. Kresse and J. Furthmuller, Comput. Mater. Sci. **6**, 15 (1996).
[98]G. Kresse and J. Furthmuller, Phys. Rev. B **54**, 11169 (1996).
[99]G. Kresse and J. Hafer, J. Phys.: Condens. Matter **6**, 8245 (1994).
[100]J. P. Perdew, J. A. Chevary, S. H. Vosko, K. A. Jackson, M. R. Pederson, D. J. Singh, and C. Fiolhais, Phys. Rev. B **46**, 6671 (1992).
[101]D. Vanderbilt, Phys. Rev. B **41**, 7892 (1990).
[102]J. H. McCreery and G. Wolken, J. Chem. Phys. **63**, 2340 (1975).
[103]J. H. McCreery and G. Wolken, J. Chem. Phys. **67**, 2551 (1977).
[104]J. Dai and J. Z. H. Zhang, J. Chem. Phys. **102**, 6280 (1995).
[105]A. Forni, G. Wiesenekker, E. J. Baerends, and G. F. Tantardini, J. Phys.: Condens. Matter **7**, 7195 (1995).